Appl. Phys. A (2016) 122:297
DOI 10.1007/s00339-016-9812-5

Applied Physics A
Materials Science & Processing

CrossMark

Photoresponse and photocapacitor properties of Au/AZO/p-Si/Al diode with AZO film prepared by pulsed laser deposition (PLD) method

A. Alyamani[1] · A. Tataroğlu[2] · L. El Mir[3,4] · Ahmed A. Al-Ghamdi[5] · H. Dahman[4] · W. A. Farooq[6] · F. Yakuphanoğlu[5,7]

Received: 2 December 2015 / Accepted: 16 February 2016 / Published online: 7 March 2016
© Springer-Verlag Berlin Heidelberg 2016

Abstract The electrical and photoresponse properties of Au/nanostructure AZO/p-Si/Al diode were investigated. Al-doped ZnO (AZO) thin films were deposited via pulsed laser deposition method on silicon substrate. Structural properties of the films were performed by using transmission electron microscopy and X-ray powder diffraction (XRD). The XRD patterns showed that the AZO films are polycrystalline with hexagonal wurtzite structure preferentially oriented in (002) direction. Electrical and photoresponse properties of the diode were analyzed under in a wide range of frequencies and illumination intensities. It is observed that the reverse current of the diode increases with increasing illumination intensity. This result confirms that the diode exhibits both photoconducting and photovoltaic behavior. Also, the transient photocurrent, photocapacitance and photoconductance measured as a function of time highly depend on transient illumination. In addition, the frequency dependence of capacitance and conductance is attributed to the presence of interface states.

✉ F. Yakuphanoğlu
fyhan@hotmail.com

1 National Nanotechnology Research Centre, KACST, Riyadh, Saudi Arabia

2 Department of Physics, Faculty of Science, Gazi University, Ankara, Turkey

3 Department of Physics, College of Sciences, Al Imam Mohammad Ibn Saud Islamic University (IMSIU), Riyadh 11623, Saudi Arabia

4 Laboratory of Physics of Materials and Nanomaterials Applied at Environment (LaPhyMNE), Faculty of Sciences, Gabes University, Gabès, Tunisia

5 Physics Department, Faculty of Science, King Abdulaziz University, Jeddah, Saudi Arabia

6 Physics and Astronomy Department, College of Science, King Saud University, Riyadh, Saudi Arabia

7 Department of Physics, Faculty of Science, Fırat University, Elazig, Turkey

1 Introduction

Transparent conducting oxides (TCOs) are metal oxides with high electrical conductivity, high optical transparency and low optical absorption. They are used in optoelectrical devices such as solar cells, flat panel displays, organic light emitting diodes, phototransistor, sensors and p–n heterojunctions [1–4]. TCOs can be classified as n-type or p-type. Zinc oxide (ZnO) is an n-type semiconductor material with wide-band gap ($\sim$3.3 eV), large exciton binding energy (60 meV) and hexagonal wurtzite structure. Doped and undoped ZnO films are a TCO and have been widely used for optoelectronic and energy conversion applications [5–7]. Especially, Al-doped ZnO (AZO) films have been used as transparent conducting metal oxide due to their high luminous transmittance and good electrical conductivity. AZO films have low resistivity, wide-band gap and good optical transmission in the visible and near-infrared regions [2, 7–9]. Also, the AZO is an n-type semiconductor material, and its free-electron concentration is usually in the range of 10^{19}–10^{21} cm^{-3} due to the extrinsic Al dopant [10].

Metal-doped ZnO thin films are prepared using different deposition techniques such as radio frequency sputtering, sol–gel spin coating, thermal oxidation, chemical vapor deposition, molecular beam epitaxy (MBE), and pulsed laser deposition (PLD) [5–11]. The PLD method enables the growth of high-quality thin films of metal oxide materials at relatively low substrate temperatures compared

with other techniques. Also, the method provides synthesizing of multilayers of different compositions with high crystalline perfection. The composition of the films grown by PLD is quite close to that of the target, even for multicomponent targets [8, 12–14].

The aim of this study is to investigate the electrical and photoresponse properties of Au/AZO/p-Si/Al diode. These properties of the diode were analyzed using current–voltage (*I–V*) and capacitance/conductance–voltage (*C/G–V*) measurements.

2 Experimental details

For the deposition of AZO thin films on silicon substrate, in the first step, AZO nanopowder was prepared by a sol–gel method based on El Mir et al. [15, 16] protocol. In this process 16 g of zinc acetate dehydrate [$Zn(CH_3COO)_2 \cdot 2H_2O$] as a precursor was dissolved in 112 ml of methanol, after 10 min under magnetic stirring at room temperature, an adequate quantity of aluminum nitrate-9-hydrate [$Al(NO_3)_3$-$9H_2O$], corresponding to [Al]/[Zn] ratio of 0.03, was added. After an additional 15 min of magnetic stirring, the solution was placed in an autoclave and dried in the supercritical conditions of ethyl alcohol (EtOH). The nanopowder was pressed inside target holder (2 inches in diameter) with 300 kg/cm^2 uniaxial pressure and annealed at 400 °C for 2 h to obtain a compact target.

In second step, the previously obtained AZO target was used for the deposition of thin films on silicon substrate by pulsed laser deposition setup (PLD/MBE 2100) from PVD products and the source is KrF excimer laser ($\lambda = 248$ nm, pulse width 20 ns, and repetition rate = 10 Hz) operated at 350 mJ to ablate the target. The deposition temperature and pressure are, respectively, 300 °C and 10^{-6} Torr. The substrate–target distance was 55 mm. All PLD parameters which may contribute to the growth rate were kept constant during 30 min, operating time, and the film thickness measured by Stylus Profiler (Veeco Dektak 150) was about 400 nm.

The silicon substrate is boron-doped (100)-oriented Si substrate ($\rho = 1$–$5\ \Omega$cm, $N_A = 5 \times 10^{15}$ cm^{-3}) with mirror-polished surface. Before deposition, for cleaning, the wafer was etched in a 10 % HF for 5 min in order to remove the eventual oxide layer that may form during storage, then rinsed in deionized water and dried with filtered N_2.

After the AZO thin film deposition process on the Si substrate, high purity (99.999 %) aluminum (Al) was deposited on the whole back of the Si wafer in the high vacuum metal evaporation system at about 10^{-7} Torr. In order to get a low resistivity ohmic contact, the Si wafer was annealed at about 570 °C for 5 min in N_2 atmosphere. Then, the front of the rectifier/Schottky contact was formed by evaporating of high purity (99.999 %) gold (Au) metal on AZO film in the same vacuum metal evaporation system.

The *I–V* measurements of Au/AZO/p-Si/Al diode were taken using a Keithley 4200 semiconductor characterization system in dark and under illumination intensity range of 10–100 mW/cm^2 using a solar simulator. The intensity of the light was measured by solar power meter (Model TM-206). The *C–V* and *G–V* measurements were taken using Keithley 4200 semiconductor characterization system in a wide frequency range.

3 Results and discussion

3.1 Structural properties

Figure 1 shows typical TEM photograph of ZnO:Al (3 at.%) aerogel nanoparticles. TEM image indicates very small particles having size in the nanometer range with prismatic-like shape and a narrow particle size distribution. The nanoparticles in the powders have approximately the same shape with a size of about 30 nm [17].

Figure 2 shows the X-ray diffraction (XRD) patterns of 3 at.% AZO aerogel nanopowder. As seen, the XRD patterns of the nanoparticles have peaks corresponding to (100), (002), (101), (102), (110), (103), (112) and (021) planes. The observed diffraction peaks correspond to the main diffraction peaks of ZnO with hexagonal wurtzite structure. No secondary phase was detected.

Figure 3 shows the typical XRD of AZO thin film deposited on silicon substrate by PLD. After deposition on silicon, the observed diffraction peaks are oriented in (002) and (400) direction. The (002) and (400) direction corresponds to the main peak of zinc oxide and silicon,

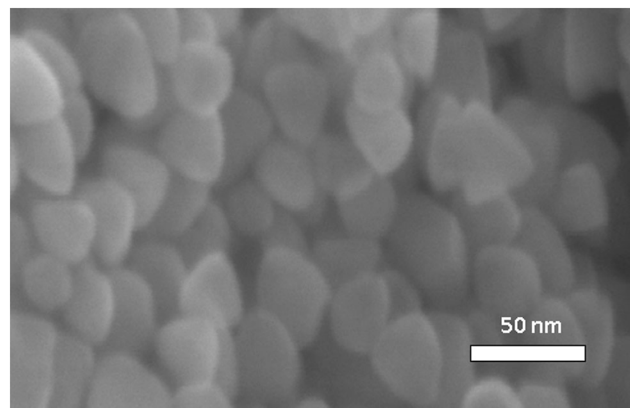

Fig. 1 Typical TEM photograph showing the general morphology of ZnO:Al (3 at.%) aerogel nanoparticles

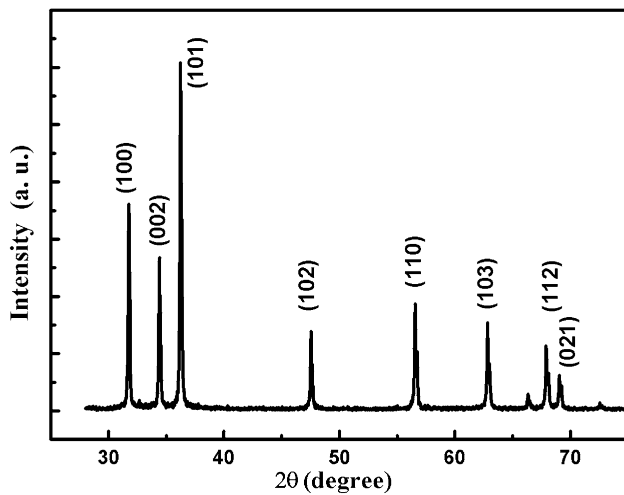

Fig. 2 X-ray diffraction of 3 at.% Al-doped ZnO aerogel nanoparticles

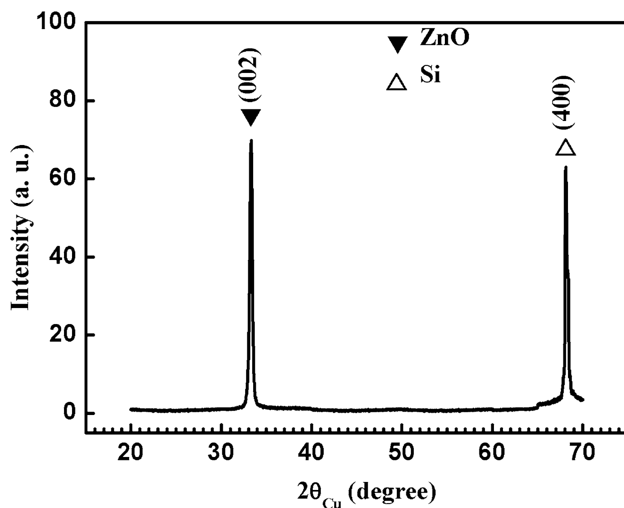

Fig. 3 Typical X-ray diffraction of AZO thin film deposited on silicon substrate by PLD

respectively. This (002) preferred orientation is due to the minimal surface energy which the hexagonal structure, c-plane to the ZnO crystallites, corresponds to the densest packed plane.

It is well known that AZO thin films deposed by PLD are highly textured in the *c* axis perpendicular to the substrate surface, especially in the (002) orientation, as shown in Fig. 3. The origin of this texture is based on the polar nature of the ZnO (002) plane, the minimal surface energy in this direction and on the high growth kinetic along the *c* axis [18, 19]. The diffraction lines of AZO films deposited on p-type silicon substrates are shown in Fig. 3. Only the (002) diffraction peak is observed, without any second phase and it is located at $2\theta = 33.26°$. This means that the films are polycrystalline with a hexagonal structure and a preferred orientation with *c* axis perpendicular to the substrates. The small deviation of (002) peak indicated that some residual stress inside the film may exist, which is characteristic for films prepared by PLD. However, some ZnO films are reported to have tensile lattice stress along the *c* axis [20, 21]. The origin of the stress can be attributed to structural imperfections at the substrate and AZO interface, which is reflected in the asymmetry of the diffraction line. The peak observed at 68.23° corresponds to (400) plane of the silicon substrate.

3.2 Current–voltage (*I–V*) measurements

The current–voltage (*I–V*) measurements have been used to extract electrical parameters of Schottky diode. The experimental *I–V* curves could be analyzed on the basis of conventional thermionic emission model. According to the TE model, the *I–V* characteristics are given by the relation [22, 23]

$$I = I_0 \exp\left(\frac{q(V - IR_s)}{nkT}\right)\left[1 - \exp\left(-\frac{q(V - IR_s)}{kT}\right)\right] \quad (1)$$

where q is the electron charge, V is the applied bias voltage, R_s is the series resistance, T is the absolute temperature, n is the ideality factor, k is the Boltzmann's constant, A is the diode contact area, and I_0 is the reverse saturation current. I_0 is derived from the straight line intercept of $\ln(I)$ at zero bias and is given by

$$I_0 = AA^* \, T^2 \, \exp\left(-\frac{q\Phi_b}{kT}\right) \quad (2)$$

where Φ_b is the barrier height at zero bias, A^* is the Richardson constant which is equal to 32 $A/cm^2\,K^2$ for p-type silicon. The value of Φ_b is obtained using the equation. For values of V greater than 3 kT/q, the ideality factor (n) can be derived from the slope of the linear region of the forward bias $\ln(I)$–V plots and is can be written as

$$n = \frac{q}{kT}\left(\frac{\mathrm{dV}}{\mathrm{d}(\ln I)}\right) \quad (3)$$

Figure 4 shows the semi-logarithmic *I–V* characteristics of the Au/AZO/p-Si/Al diode under dark and various illumination intensities. It is clear from this figure that the diode exhibited an illumination sensitive behavior. It was found that the reverse current increases with illumination intensity for a given reverse voltage and is higher than the dark current. This indicates that the diode exhibits a photodiode behavior. When a photon of sufficient energy strikes the diode, it creates an electron–hole pair. The free carriers generated by photons can lead to an increase in reverse current depending on the number of generated electron–hole pairs [24–28]. Also, the forward current of the diode

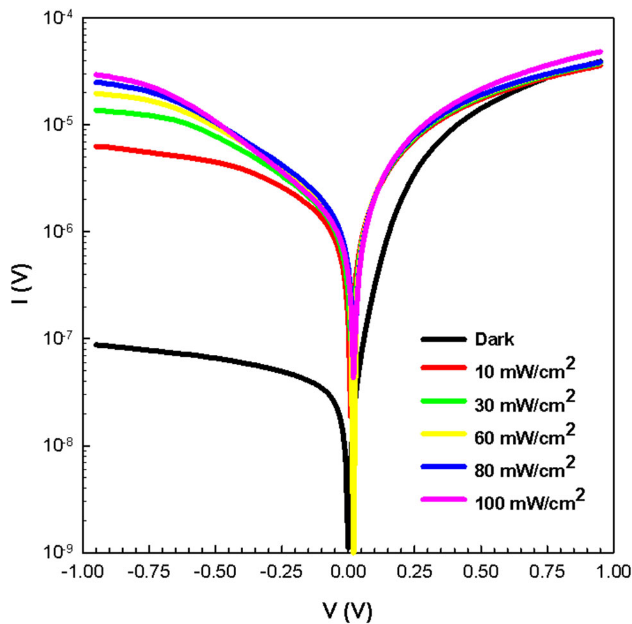

Fig. 4 The semi-logarithmic *I–V* characteristics of the diode under dark and various illumination intensities

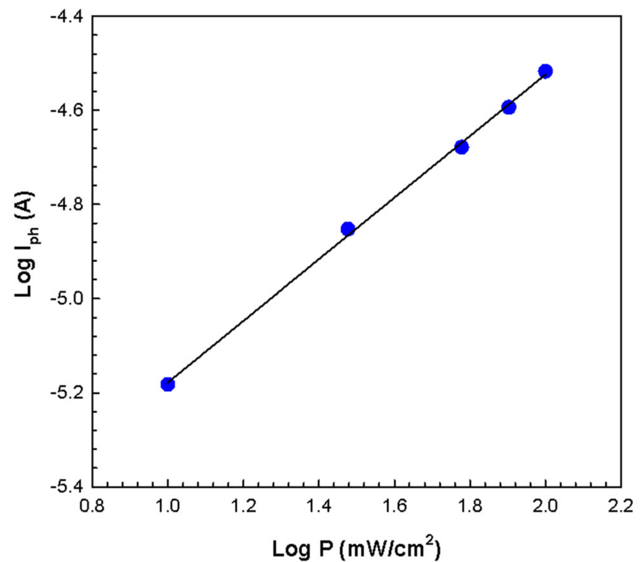

Fig. 5 Plot of log(I_{ph}) versus log(P) of the diode (at −1 V)

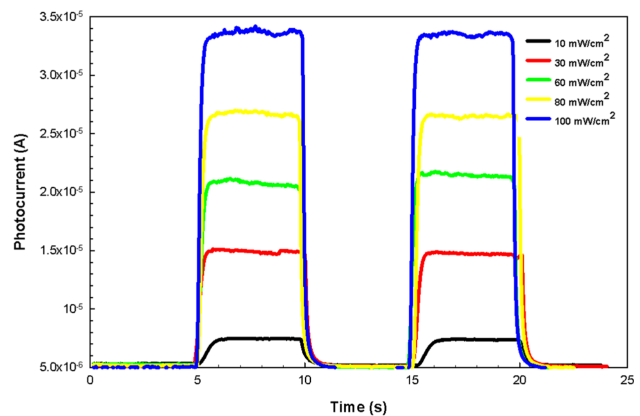

Fig. 6 Plots of transient photocurrent-time of the diode at various illumination intensities and 1 V

deviates from the linear *I–V* behavior which could be due to presence of series resistance and interface states [29–33].

The barrier height and ideality factor values of the diode were found to vary in the range of 0.71–0.64 and 1.78–2.86 eV, respectively. This behavior of n is attributed to the presence of thin film layer, inhomogeneities of the barrier height, interface states, and series resistance [29–36].

In addition, the photoconduction mechanism of the Au/AZO/p-Si/Al diode was investigated. The variation in the photocurrent with illumination was analyzed by the following equation [37, 38],

$$I_{ph} = BP^{m} \tag{4}$$

where I_{ph} is the photocurrent, P is the illumination intensity, B is a constant, and m is an exponent. The m value in the range of 0.5–1 implies that the photoconducting mechanism is controlled by the presence of continuous distribution of trap levels. Figure 5 shows the photocurrent plot of the diode at −1 V. The value of m was determined from the slope of log(I_{ph}) versus log(P) plot, and it was found to be 0.65. The obtained m value indicates that the photocurrent exhibits a linear behavior. As a result, the diode could be used as a photodiode in various optoelectronic applications.

3.3 Transient photocurrent, photocapacitance and photoconductance measurements

The transient photocurrent-time measurements are a well-known technique for the analysis of photoconducting mechanism. Figure 6 shows the plots of photocurrent of the diode at various illumination intensities at 1 V. As seen in Fig. 6, the photocurrent of the diode increases rapidly up to certain level with switching on of the illumination and then, it comes back to initial level with switching off. The increase in photocurrent is due to the number of photo-generated charge carriers in the depletion region of the diode. The decrease in photocurrent is due to the trapping of the charge carriers in the deep levels; thus coming back to its initial state [39–44]. Also, the magnitudes of the photocurrent at every on/off cycle are steady and reproducible. The photoresponse results indicate that the diode can be used as a photodiode.

When the light is applied to a diode, the photo-induced charges are produced and most of the charges are constituted by holes. The transient time (τ_T) and the photocharge density (ρ_{ph}) are given by

$$\tau_T = \frac{d^2}{2\mu V} \quad \text{and} \quad \rho_{ph} = \frac{2J_{ph}\tau_T}{d} \tag{5}$$

where J_{ph} is the photocurrent density, μ is the mobility and d is the depletion width. The transient photocapacitance is a measure of the density of photogenerated carriers in the space charge region [45–47]. The photocapacitance is given as

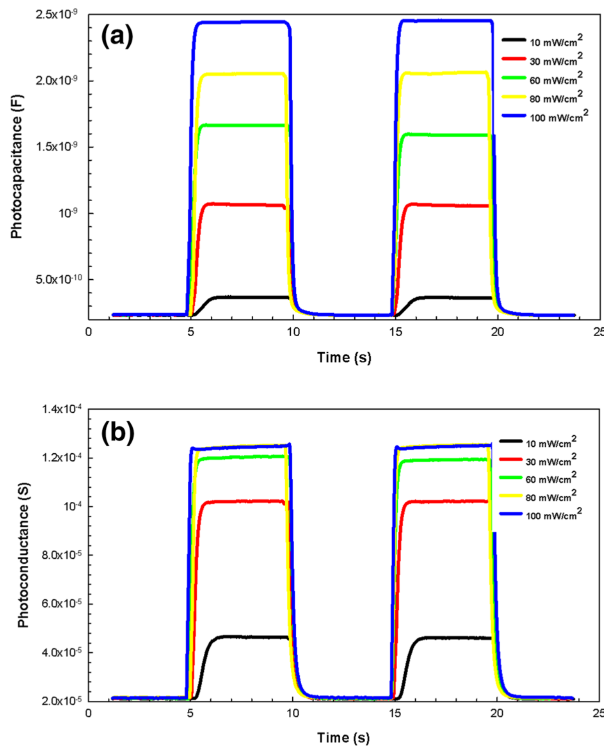

Fig. 7 Plots of **a** photocapacitance-time, **b** photoconductance-time plots of the diode at various illumination intensities and 10 kHz

$$C_{\mathrm{ph}} = -\frac{\mathrm{d}\sigma_{\mathrm{ph}}}{\mathrm{d}V} = -\frac{d}{2}\frac{\mathrm{d}\rho_{\mathrm{ph}}}{\mathrm{d}V} \tag{6}$$

Figure 7a, b show the plots of transient photocapacitance-time and photoconductance-time of the diode at various illumination intensities and 10 kHz, respectively. As seen in these figures, the value of photocapacitance and photoconductance increases with increasing illumination intensity. On illuminating the diode, the photocapacitance and photoconductance of the diode increase rapidly to a constant value and then decrease to original value after turning off the illuminating. This increase could be due to the increase in number of photogenerated charge carriers at in interface states. This decrease is due to transfer of the photogenerated charge carriers back to the original level [24, 26, 28, 40, 48, 49].

3.4 Capacitance/conductance–voltage (*C*/*G*–*V*) measurements

Figure 8a, b shows the plots of capacitance–voltage and conductance–voltage of the diode in the frequency range of 10 kHz–1 MHz. As seen in Fig. 8a, the capacitance value of the diode does not change with frequency at the positive bias voltages, but it increases with increasing frequency at the negative bias voltages. The frequency dependence of the capacitance is due to the presence of interface states at the interface of AZO/Si. At low frequencies, the interface states can follow the alternating current (ac) signal and can contribute to the total capacitance. At high frequencies, the interface states cannot follow the ac signal and cannot contribute to the total capacitance [50–56]. As seen from Fig. 9, the conductance value increases with increasing

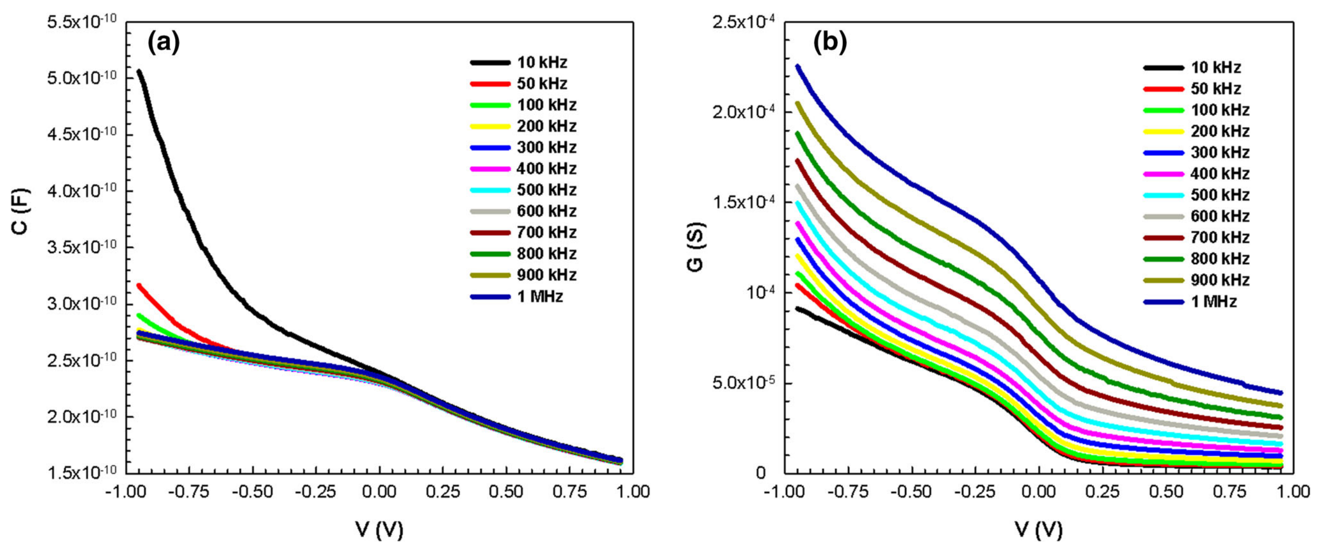

Fig. 8 Plots of **a** capacitance–voltage (*C*–*V*), **b** conductance–voltage (*G*–*V*) of the diode at various frequencies

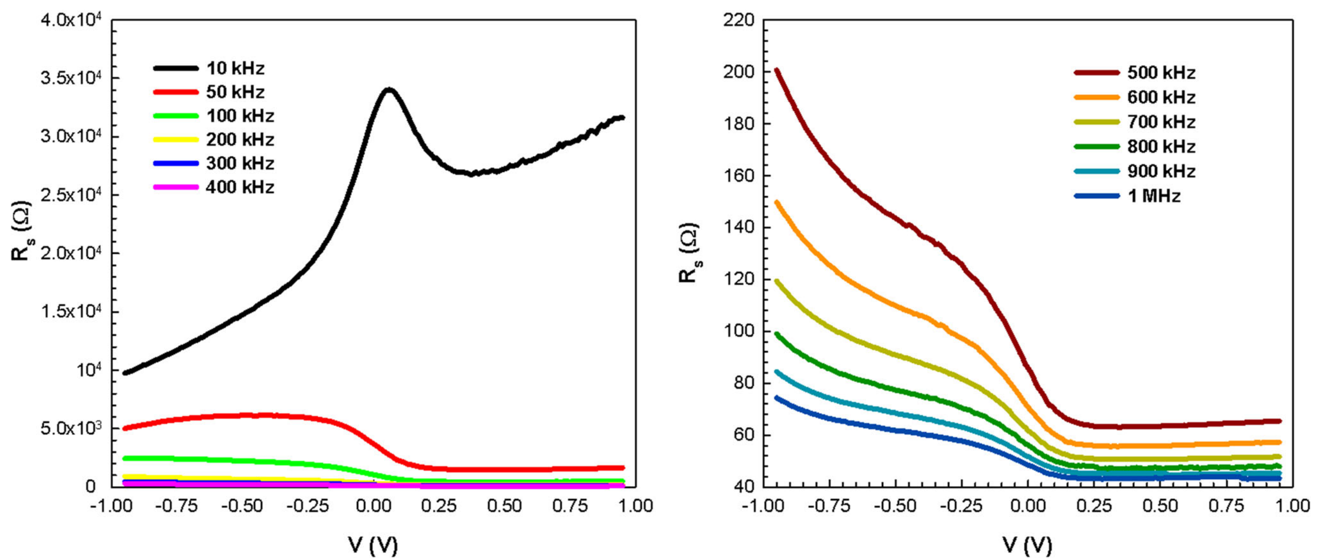

Fig. 9 Plots of series resistance–voltage (R_s–V) of the diode at various frequencies

frequency. This behavior of conductance is attributed to the presence of the interface states.

The series resistance (R_s) is an important parameter causing deviation from ideal diode behavior. The R_s can be determined using conductance method developed by Nicollian and Goetzberger [29]. According to this method, the R_s is expressed by the following equation,

$$R_s = \frac{G_{ma}}{G_{ma}^2 + (\omega C_{ma})^2} \tag{7}$$

where C_{ma} and G_{ma} are the measured capacitance and conductance, respectively. Figure 9 shows the plots of series resistance versus voltage of the diode in the frequency range of 10 kHz–1 MHz. As seen in Fig. 9, the calculated R_s value decreases with increasing frequency. This behavior of R_s is a result of frequency-dependent charges such as interface charge, fixed/mobile oxide charge, and oxide-trapped charge. Furthermore, at only 10 kHz, the R_s plot gives a peak in the range of 0–0.25 V, and this peak disappears with increasing frequency. The presence of this peak is attributed to the change in interface states. At low frequencies, the interface states can follow frequency of alternating current applied [50–56].

4 Conclusions

AZO thin films were deposited on silicon substrate at 300 °C by PLD from Al-doped zinc oxide target based on nanocrystalline powder synthesized by sol–gel method. The films exhibited (002) hexagonal *c* axis preferred orientation perpendicular to the substrate. The transient photocurrent, photocapacitance and photoconductance measurements were used to analyze the photoresponse of the diode. It is found that the obtained component shows good photoresponse behavior. In addition, the *C*–*V* and *G*–*V* characteristics of the diode confirm that both the *C* and *G* values vary with applied voltage and frequency. The obtained results suggest that the fabricated diode can be used as a photodiode or photocapacitor in optoelectronic applications.

Acknowledgments Two of the authors thank King Saud University for support.

References

1. A. Stadler, Materials **5**, 661–683 (2012)
2. A.A. Al-Ghamdi, O.A. Al-Hartomy, M. El Okr, A.M. Nawar, S. El-Gazzar, F. El-Tantawy, F. Yakuphanoglu, Spectrochim. Acta Part A Mol. Biomol. Spectrosc. **131**, 512–517 (2014)
3. D.O. Scanlon, K.G. Godinho, B.J. Morgan, G.W. Watson, J. Chem. Phys. **132**, 024707–024710 (2010)
4. S. Ruzgar, S. Aksoy, J. Mater. Electron. Devices **1**, 38–41 (2015)
5. J.-P. Kim, J.-S. Bae, J.-K. Bang, J.-H. Yoon, M.-S. Won, B.S. Lee, S.-Y. Lee, O.-S. Jung, E. Kim, J. Korean Phys. Soc. **56**, 378–382 (2010)
6. M. Dosmailov, L.N. Leonat, J. Patek, D. Roth, P. Bauer, M.C. Scharber, N.S. Sariciftci, J.D. Pedarnig, Thin Solid Films **591**, 97–104 (2015)
7. M. Alauddin, J.K. Song, S.M. Park, Appl. Phys. A **101**, 707–711 (2010)
8. H. Kim, A. Piqué, J.S. Horwitz, H. Murata, Z.H. Kafafi, C.M. Gilmore, D.B. Chrisey, Thin Solid Films **377–378**, 798–802 (2000)
9. J.H. Lee, T. Lu, S. Cho, F. Khatkhatay, L. Chen, H. Wang, Thin Solid Films **524**, 320–327 (2012)
10. X.D. Li, T.P. Chen, Y. Liu, K.C. Leong, Opt. Express **22**, 23086–23093 (2014)
11. M. Benhaliliba, C.E. Benouis, M.S. Aida, F. Yakuphanoglu, A. Sanchez Juarez, J. Sol Gel Sci. Technol. **55**, 335–342 (2010)

12. F.K. Shan, Y.S. Yu, J. Eur. Ceram. Soc. **24**, 1869–1872 (2004)
13. A. Suzuki, T. Matsushita, N. Wada, Y. Sakamoto, M. Okuda, Jpn. J. Appl. Phys. **35**, L56–L59 (1996)
14. F.K. Shan, B.C. Shin, S.C. Kim, Y.S. Yu, J. Korean Phys. Soc. **42**, S1374–S1377 (2003)
15. L. El Mir, A. Amlouk, C. Barthou, S. Alaya, Phys. B **388**, 412–417 (2007)
16. L. El Mir, J. El Ghoul, S. Alaya, M. Ben Salem, C. Barthou, H.J. von Bardeleben, Phys. B Condens. Matter **403**, 1770–1774 (2008)
17. M. Hjiri, L. El Mir, S.G. Leonardi, Chemosensors **2**, 121–130 (2014)
18. L. El Mir, Z. Ben Ayadi, M. Saadoun, H.J. von Bardeleben, K. Djessas, A. Zeinert, Phys. Status Solidi (A) **204**, 3266–3277 (2007)
19. L. El Mir, Z. Ben Ayadi, M. Saadoun, K. Djessas, H.J. von Bardeleben, S. Alaya, Appl. Surf. Sci. **254**, 570–573 (2007)
20. E.M. Bachari, G. Baud, S. Ben Amor, M. Jacquet, Thin Solid Films **348**, 165–172 (1999)
21. V. Gupta, A. Mansingh, J. Appl. Phys. **80**, 1063–1073 (1996)
22. A. Dere, J. Mater. Electron. Devices **1**, 7–10 (2015)
23. S. Altındal, J. Mater. Electron. Devices **1**, 7–10 (2015)
24. I. Yun, *Photodiodes-from Fundamentals to Applications* (InTech, Croatia, 2012)
25. A. Tataroglu, H. Tuncer, A.A. Al-Ghamdi, A. Dere, B. Arif, S. Yol, N. Ozdemir, F. El-Tantawy, F. Yakuphanoglu, Synth. Metals **206**, 15–23 (2015)
26. I.A. Elsayed, M. Cavas, R. Gupta, T. Fahmy, A.A. Al-Ghamdi, F. Yakuphanoglu, J. Alloys Compd. **638**, 166–171 (2015)
27. I. Beinik, M. Kratzer, A. Wachauer, L. Wang, Y.P. Piryatinski, G. Brauer, X.Y. Chen, Y.F. Hsu, A.B. Djuriši, C. Teichert, Beilstein J. Nanotechnol. **4**, 208–217 (2013)
28. H. Aydın, A. Tataroglu, A.A. Al-Ghamdi, F. Yakuphanoglu, F. El-Tantawy, W.A. Farooq, J. Alloys Compd. **625**, 18–25 (2015)
29. E.H. Nicollian, A. Goetzberger, Bell Syst. Tech. J. **46**, 1055–1133 (1967)
30. R.T. Tung, Phys. Rev. B **64**, 205310 (2001)
31. S.H. Kim, C.Y. Jung, H. Kim, Trans. Electr. Electron. Mater. **15**, 324–327 (2014)
32. R. Padma, V. Rajagopal Reddy, Adv. Mater. Lett. **5**, 31–38 (2014)
33. A. Tataroglu, A.A. Al-Ghamdi, S. Bin Omran, W.A. Farooq, F. El-Tantawy, F. Yakuphanoglu, J. Sol Gel Sci. Technol. **71**, 421 (2014)
34. R. Kumar, S. Chand, J. Mater. Sci.: Mater. Electron. **25**, 4531–4537 (2014)
35. E. Marıl, A. Kaya, H.G. Çetinkaya, S. Koçyiğit, Ş. Altındal, Mater. Sci. Sem. Process. **39**, 332–338 (2015)
36. L. Changshi, L. Feng, Comput. Mater. Sci. **107**, 170–174 (2015)
37. R. Singh, A.K. Narula, Appl. Phys. Lett. **71**, 2845–2847 (1997)
38. J.M. Lee, J.C. Shin, C.S. Hwang, H.J. Kim, J. Vac. Sci. Technol., A **16**, 2768–2771 (1998)
39. S. Wageh, A.A. Al-Ghamdi, Y. Al-Turki, A. Dere, S.C. Tjong, F. El-Tantawy, F. Yakuphanoglu, Opt. Quant. Electron. **47**, 1779–1789 (2015)
40. A.S. Dahlan, A. Tataroğlu, A.A. Al-Ghamdi, A.A. Al-Ghamdi, S. Bin-Omran, Y. Al-Turki, F. El-Tantawy, F. Yakuphanoglu, J. Alloys Compd. **646**, 1151–1156 (2015)
41. B. Varghese, B. Mukherjee, K.R.G. Karthik, K.B. Jinesh, S.G. Mhaisalkar, E.S. Tok, C.H. Sow, J. Appl. Phys. **111**, 104306 (2012). **(1–6)**
42. G. Cheng, X. Wu, B. Liu, B. Li, X. Zhang, Z. Dua, Appl. Phys. Lett. **99**, 203105 (2011). **(1–3)**
43. R.H. Al Orainy, A.A. Hendi, Microelectron. Eng. **127**, 14–20 (2014)
44. Y.-H. Chang, C.-M. Liu, Y.-C. Tseng, C. Chen, C.-C. Chen, H.-E. Cheng, Nanotech. **21**, 225602 (2010)
45. I. Nurdjaja, E.A. Schiff, Mater. Res. Soc. Symp. Proc. **467**, 723–728 (1997)
46. I.A. Elsayed, M. Cavas, R. Gupta, T. Fahmy, A.A. Al-Ghamdi, F. Yakuphanoglu, J. Alloys Compd. **638**, 166–171 (2015)
47. C. Casteleiro, R. Schwarz, U. Mardolcar, A. Maçarico, J. Martins, M. Vieira, F. Wuensch, M. Kunst, E. Morgado, P. Stallinga, H.L. Gomes, Thin Solid Films **516**, 5118–5121 (2008)
48. S. Shukla, S. Kumar, Bull. Mater. Sci. **34**, 1351–1355 (2011)
49. G.L. Miller, D.V. Lang, L.C. Kimerling, Ann. Rev. Mater. Sci. **7**, 377–448 (1977)
50. A. Tataroğlu, H. Aydın, A.A. Al-Ghamdi, F. El-Tantawy, W.A. Farooq, F. Yakuphanoglu, J. Electroceram. **32**, 369–375 (2014)
51. A. Kumar, S. Mondal, S.G. Kumar, K.S.R. Koteswara Rao, Mater. Sci. Semicon. Process. **40**, 77–83 (2015)
52. T. Ataseven, A. Tataroğlu, T. Memmedli, S. Özçelik, J. Opto-electron. Adv. Mater. **14**, 640–645 (2012)
53. M. Cavas, A.A.M. Farag, Z.A. Alahmed, F. Yakuphanoglu, J. Electroceram. **31**, 298–308 (2013)
54. S. Demirezen, A. Kaya, Ö. Vural, Ş. Altındal, Mater. Sci. Semicon. Process. **33**, 140–148 (2015)
55. Ş. Karatas, F. Yakuphanoglu, F.M. Amanullah, J. Phys. Chem. Solids **73**, 46–51 (2012)
56. M.S. Pratap Reddy, J.-H. Lee, J.-S. Jang, Synth. Metal **185–186**, 167–171 (2013)